Title

220 Year Diatom δ18O Reconstruction of the Guaymas Basin Thermocline Using Microfluorination

Journal

Paleoceanography and Paleoclimatology, 35(2)

ISSN

2572-4517

Authors

Menicucci, Anthony J
Thunell, Robert C
Spero, Howard J

Publication Date

2020-02-01

DOI

10.1029/2019pa003749

Peer reviewed

Paleoceanography and Paleoclimatology

RESEARCH ARTICLE
10.1029/2019PA003749

Special Section:
Special Collection to Honor the Career of Robert C. Thunell

220 Year Diatom $\delta^{18}O$ Reconstruction of the Guaymas Basin Thermocline Using Microfluorination

Anthony J. Menicucci[1], Robert C. Thunell[2], and Howard J. Spero[1]

[1]Department of Earth and Planetary Sciences, University of California, Davis, CA, USA, [2]School of the Earth, Ocean and Environment, University of South Carolina, Columbia, SC, USA

Abstract The removal of exchangeable oxygen from diatom opal prior to $\delta^{18}O_{diatom}$ analysis is a crucial first step before analyzing frustule oxygen isotopes for paleoceanographic applications. We present the results of experiments that quantify the temperature-dependent reactivity of biogenic silica with water under laboratory conditions. We demonstrate that controlled exchange between rinse water and diatom opal at room temperature results in predictable alteration of $\delta^{18}O_{diatom}$, after vacuum dehydroxylation. Diatom samples equilibrated with an ^{18}O-enriched $\delta^{18}O_{equil.\ water}$ solution of +94.4‰ at ~21 °C for 70 hr prior to dehydroxylation yield $\delta^{18}O_{diatom}$ data that can be directly interpreted with existing empirical $\delta^{18}O_{diatom}$ versus temperature relationships. We compare sediment trap-based $\delta^{18}O_{diatom}$ temperature data with modern $\delta^{18}O_{foram}$ temperatures. Finally, we present an ~220 year record of $\delta^{18}O_{diatom}$ data from an eastern Pacific Guaymas Basin boxcore, analyzed using the microfluorination technique, that indicates diatom chlorophyll maximum (Chl_{max}) temperatures have shifted from a period during the late eighteenth and nineteenth centuries that was 8 °C cooler during the fall bloom relative to mean annual alkenone $U^{k'}_{37}$ sea surface temperature, to the late twentieth century when we observe no difference between alkenone sea surface temperature and diatom Chl_{max}. These data suggest a twentieth century seasonal shift in the timing of fall upwelling and Guaymas Basin stratification breakdown that could be due to reduced upwelling efficiency and/or increased summer mixed layer thermal stratification.

Key Points:
- Diatom $\delta^{18}O$ data show predictable alteration at ambient laboratory temperatures due to exchange with rinse water but is correctable
- Guaymas Basin diatom sediments biased toward the fall bloom and track well with existing foraminifera data sets
- Diatom $\delta^{18}O$ temperatures record chlorophyll maximum temperatures warming by ~10°C over a 220 year time frame

Correspondence to:
A. J. Menicucci,
amenicucci@usf.edu

Citation:
Menicucci, A. J., Thunell, R. C., & Spero, H. J. (2020). 220 year diatom $\delta^{18}o$ reconstruction of the guaymas basin thermocline using microfluorination. *Paleoceanography and Paleoclimatology*, *35*, e2019PA003749. https://doi.org/10.1029/2019PA003749

Received 7 AUG 2019
Accepted 14 NOV 2019
Accepted article online 19 NOV 2019

1. Introduction

1.1. Geochemical Background

The oxygen isotopic composition of biogenic calcite and aragonite is frequently used to reconstruct past temperature and salinity conditions from the fossil record (Spero et al., 2003; Waelbroeck et al., 2005). In contrast, analyses of the oxygen isotope composition of biogenic opal from organisms such as diatoms are comparatively uncommon yet have the potential to provide similar paleoceanographic information from environments that lack carbonate material. Diatoms, composed of opal-A type silica (DeMaster & Turekian, 2003), most commonly inhabit the upper pycnocline close to the chlorophyll maximum (Chl_{max}) (Round et al., 1990; Swann et al., 2008). Because diatoms are phytoplankton, the $^{18}O/^{16}O$ of their frustules is thought to record thermocline temperatures within the photic zone as siliceous microfossils dominate the autochthonous sediment during peak seasonal blooms (Shemesh et al., 1992; Thunell, 1998). When combined with other proxies, such as $U^{k'}_{37}$ alkenone sea surface temperature (SST) and/or foraminifera $\delta^{18}O$ measurements (Goni et al., 2001; Thunell, 1998), $\delta^{18}O_{diatom}$ data have the potential to elucidate temperature gradients and/or seasonal variability across the photic zone (Spero et al., 2003; Swann et al., 2006; Swann & Leng, 2009).

A fundamental challenge for $\delta^{18}O_{diatom}$ interpretation is understanding how these data relate to depth and seasonally influenced temperature of the water column. Many empirical calibrations have been published that relate the $\delta^{18}O$ of inorganic and biogenic silica to temperature (Brandriss et al., 1998; Clayton et al., 1972; Crespin et al., 2010; Dodd & Sharp, 2010; Kawabe, 1978; Knauth & Epstein, 1976; Labeyrie, 1974; Leclerc & Labeyrie, 1987; Moschen et al., 2005; Sharp et al., 2016; Sharp & Kirschner, 1994; Zheng et al., 1994), with these relationships utilizing a range of silica mineralogies including amorphous silica, biogenic opal, and quartz. In the range of environmentally relevant temperatures (0–30 °C), these calibrations yield $10^3 ln\alpha_{silica\text{-}water}$ values that are >10‰ different from each other for the same temperatures (Brandriss et al., 1998; Crespin et al., 2010; Dodd & Sharp, 2010). In addition, marine and freshwater diatom calibrations exhibit significant differences in the empirical temperature relationships that preclude

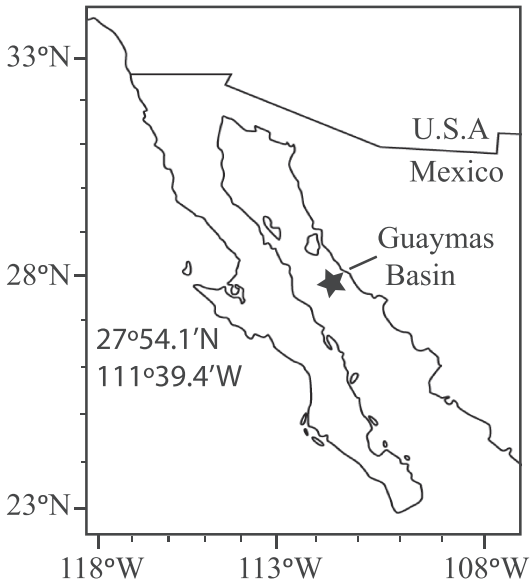

Figure 1. Location of the Guaymas Basin sediment trap series (STS) and sediment core BC-43 in the Gulf of California (27°54.05′N, 111°39.43′W) is identified with a star. Note that the locations of the STS and BC-43 box core sites are nearly identical; both are covered by the star symbol.

their broad application across different environments (Brandriss et al., 1998; Dodd et al., 2012; Dodd & Sharp, 2010; Moschen et al., 2005). Sharp et al. (2016) demonstrated that biogenic opal falls along the same $^{18}O/^{16}O$ and $^{17}O/^{16}O$ fractionation lines as quartz samples from higher temperatures, yet they still had to account for a data spread (>4‰ for similar calculated temperatures) in the previously published $\delta^{18}O_{diatom}$ data sets that were calibrated at lower temperatures. As such, researchers often must make a qualitative choice in selecting one of many $\delta^{18}O_{diatom}$ versus temperature relationships in order for their data to yield environmentally realistic results for a given location.

The presence of hydroxyl and other exchangeable oxygen in the diatom opal lattice likely contributes to the range of values observed. However, some of the methods employed to remove these exchangeable oxygen sources prior to isotope ratio mass spectrometer (IRMS) analysis affect $\delta^{18}O_{diatom}$ data in repeatable and predictable ways. For instance, the Controlled Isotope Exchange procedure (Labeyrie et al., 1988; Labeyrie & Juillet, 1982; Leclerc & Labeyrie, 1987) exposes diatom samples to ^{18}O-enriched water vapor at a constant temperature while under vacuum in order to label and stabilize the isotopic composition of the exchangeable oxygen prior to a dehydroxylation procedure. A comparable method was recently proposed by Menicucci et al. (2017), where previously cleaned diatom samples were exposed to an ^{18}O-enriched rinse solution during the final sample preparation stage. These authors presented data further illustrating that diatom samples undergo a reproducible and predictable isotopic exchange with the $\delta^{18}O_{equil.\ water}$ solutions and that the effect of this exchange persists after vacuum dehydroxylation. Among the testable hypotheses proposed by Menicucci et al. (2017) was the possibility that some of the offsets between oxygen isotope analytical methodologies could arise from using rinse waters with different geochemistries prior to IRMS analysis. Dodd et al. (2017) also demonstrated the effects of exchangeable oxygen in the diatom frustules, and showed that as exchangeable oxygen decreases, the diatom $\delta^{18}O$ values are permanently altered.

1.2. Guaymas Basin, Gulf of California

The Guaymas Basin (GB) in the Gulf of California (Figure 1) is an extensively studied location where more than two decades of environmental data and prior field campaigns have constrained seasonal water column hydrography, thereby providing important context for the interpretation of $\delta^{18}O_{diatom}$ data (Goni et al., 2001; Goni et al., 2006; Thunell, 1998). Between May and September, the upper surface waters of the GB photic zone are thermally stratified, with low primary productivity and maximum peak summer temperatures approaching 30 °C (Goni et al., 2001; Thunell, 1998; Thunell et al., 1993; Thunell et al., 1994; Thunell et al., 1996).

At the peak of September thermal stratification, the mixed layer reaches ~45 m depth and intersects with the upper region of the Chl_{max} (Goni et al., 2001; Thunell, 1998). In October, stratification starts to break down as the western North American subtropical high migrates southward (Cheshire et al., 2005; Wejnert et al., 2010). This atmospheric shift generates NW winds that drive upwelling and produce a shoaling of the thermocline. Phytoplankton productivity, particularly from diatoms, increases with nutrient availability (Goni et al., 2001; Thunell, 1998; Thunell et al., 1996; Wejnert et al., 2010) as waters upwell, and seasonal foraminifera make their appearance in the thermocline (Davis et al., 2019; Wejnert et al., 2010). Peak biogenic opal production in the GB occurs during this fall bloom when the Chl_{max} is part of the lower mixed layer/upper thermocline, between 30 and 45 m depth (Goni et al., 2001; Thunell, 1998; Wejnert et al., 2010). Although upwelling persists, by mid-January the upper 100 m of the water column has cooled to below 15 °C and the fall diatom bloom ends (Davis et al., 2019; Goni et al., 2001; Thunell, 1998; Wejnert et al., 2010).

In this study, we present experimental data that supports a sample preparation method to be used prior to vacuum dehydroxylation and sample microfluorination that yields reproducible $\delta^{18}O$ data that can be

interpreted with existing marine temperature calibrations. Utilizing our methodology, we analyze sediment trap and fossil diatom material from a GB boxcore that was the subject of previous alkenone and flux studies (Goni et al., 2001; Goni et al., 2006). Our results allow us to constrain the seasonality of fossil diatoms in the sediment, directly compare our sediment trap data to thermocline dwelling nonspinose foraminifera data, and to reconstruct upper water column thermal structure changes across the past 220 years. Finally, we compare $\delta^{18}O_{diatom}$ data, interpreted as Chl_{max} temperatures, with SST reconstructions derived from alkenone $U^{k'}_{37}$ data to produce a comprehensive, non-$CaCO_3$ sourced, interpretation of mixed layer/upper thermocline hydrography during this time interval.

2. Methods

2.1. Sample Location

Samples were obtained from the GB, Gulf of California (27°54.05′N, 111°39.43′W) (Figure 1), which is the site of a long-term sediment trap time series (STS) (~500 m depth) (Thunell, 1998), with bi-weekly sample collection via an automated system within the trap mechanism (Davis et al., 2019). We selected seven STS samples across one full year from the beginning of the 1996 fall bloom between 27 October and 10 November through the summer of 1997. One of these samples, STS-1, had sufficient material to conduct equilibration experiments. In addition, we selected 15 recent intervals from box-core BC-43 (Table 1), which was collected approximately 2.5 km SW of the STS mooring. BC-43 samples were purified from residual freeze dried sediment analyzed in previous $U^{k'}_{37}$ alkenone studies (Goni et al., 2001; Goni et al., 2006). The age model is based on excess ^{210}Pb (Pride, 1997), suggesting a sedimentation rate of ~12 cm/century during the sampled interval. This sedimentation rate, in conjunction with the sediment core collection date, was used to calculate sample ages (Goni et al., 2001).

2.2. Sample Cleaning and Purification

We follow the sample cleaning procedures detailed in Menicucci et al. (2017). Briefly, organics were removed by reacting sediment samples in 30% H_2O_2 at ambient temperature (21.2 °C, ±0.3 °C) for 24 hr, and then heating to 90 °C for 6–8 hr to react the remaining organic material to completion. The supernatant was then decanted and washed in 18 MΩ deionized water (DI), and subsequently soaked in 5% HCl for 15 hr to remove all carbonate material. Samples were subsequently decanted, triple rinsed in DI, and the 10–75 μm sieve fraction was isolated and centrifuged in DI water to differentially settle clay from biogenic opal (diatom frustules). The separated biogenic opaline fraction was pipetted by hand into 10 ml centrifuge tubes containing a solution of liquid sodium polytungstate (SPT; sp. gr. = 2.08 gm cm^3) and centrifuged at 2,000 rpm to partition the residual clay contaminants and diatom frustules. The cap of isolated diatom material was then collected and rinsed with DI several times to remove all SPT residue, dried at 90 °C for 1 hr, then stored in a vacuum desiccator. All sediment trap samples other than STS-1, were cleaned in this manner and were not exposed to an ^{18}O-enriched $\delta^{18}O_{equil.\ water}$ solution, as described below.

2.3. Equilibration Experiments Between Diatoms and Water

We quantified the equilibration between exchangeable oxygen in the diatom opal lattice by immersing samples of STS-1 and a BC-43 sample from 11 cm core depth in two different equilibration waters with $\delta^{18}O_{equil.\ water} = -8.2‰$, and +94.4‰ at a laboratory temperature of 21.2 °C (±0.3 °C) for 70 hr. This matches the temperature conditions and duration that diatom samples encounter during cleaning and purification in a typical laboratory. We note that similar experiments conducted by Menicucci et al. (2017) at 90 °C demonstrated that the shift in $\delta^{18}O_{diatom}$ covaries linearly with changing $\delta^{18}O_{equil.\ water}$ values. Hence we can quantify the slope of this relationship at room temperature with just two equilibration waters.

All remaining fossil diatom samples from BC-43 core intervals (Table 1) were soaked in the $\delta^{18}O_{equil.\ water}$ solution of +94.4‰ prior to vacuum dehydroxylation and IRMS analysis in order to produce $\delta^{18}O_{diatom}$ data that could be directly applied to previously established diatom $\delta^{18}O$ versus temperature relationships (see section 4.2). Equilibration water $\delta^{18}O$ values were quantified with a Laser Water Isotope Analyzer V2 (Los Gatos Research Inc., Mountain View, CA) (1σ precision ranging between ±0.15‰ and 0.30‰). Ten milliliters of isotopically distinct water was added to approximately 5 mg of each purified diatom sample in two 20 ml scintillation vials. Scintillation vials were capped with conical polyseal inserts and placed in a cabinet for 70 hr. After, the labeled water was decanted, and the diatom samples were dried at 90 °C

Table 1
Measured $\delta^{18}O_{diatom}$ After Equilibration With $\delta^{18}O_{equil.\ water}$ Solutions

			$\delta^{18}O_{diatom}$ equilibrated at 21.2°C[b]					
Sample name	Depth (cm)	Date (CE)[a]	−8.2‰	+94.4‰	% mass loss[c]	$\delta^{18}O_{diatom}$ temperature[d,e]	$U^{k'}_{37}$ temperature[f]	ΔT $\delta^{18}O$-$U^{k'}_{37}$
STS-0	Sediment trap	27 Oct 1996	31.3	—	10.3	27.3	—	—
STS-1	Sediment trap	10 Nov 1996	32.2	35.9	13.0	22.3	—	—
STS-2	Sediment trap	22 Dec 1996	32.5	—	10.8	21.8	—	—
STS-3	Sediment trap	2 Feb 1997	32.8	—	14.3	20.5	—	—
STS-4	Sediment trap	6 Apr 1997	32.1	—	15.0	23.6	—	—
STS-5	Sediment trap	1 June 1997	31.3	—	10.7	27.3	—	—
STS-6	Sediment trap	24 Aug 1997	32.0	—	13.6	24.1	—	—
BC-43	1.5	1979	—	37.4	11.0	25.5	23.9	1.6
BC-43	3.0	1966	—	38.4	10.7	21.0	24.1	−3.1
BC-43	4.0	1958	—	38.7	11.2	20.0	24.3	−4.3
BC-43	6.5	1936	—	39.0	11.0	19.0	24.4	−5.4
BC-43	10.0	1906	—	38.4	9.3	21.0	24.2	−3.2
BC-43	11.0	1897	35.8	38.1	9.7	22.1	24.6	−2.5
BC-43	13.5	1876	—	39.3	10.4	17.9	24.1	−6.2
BC-43	15.5	1859	—	39.2	10.2	18.3	24.4	−6.1
BC-43	17.0	1846	—	39.5	9.2	17.2	23.8	−6.6
BC-43	18.0	1837	—	39.2	10.0	18.3	24.0	−5.7
BC-43	20.5	1815	—	39.6	10.5	16.9	23.5	−6.6
BC-43	22.5	1798	—	39.3	11.2	17.9	23.3	−5.4
BC-43	24.0	1785	—	40.1	10.9	15.2	22.3	−7.1
BC-43	25.0	1777	—	40.0	11.1	15.5	22.1	−6.6
BC-43	27.0	1759	—	39.5	10.9	17.2	20.8	−3.6
NBS 28	—	—	—	—	0.5	—	—	—

[a]All age data are in years (CE). See Goni et al. (2001) for core age model. [b]$\delta^{18}O$ data are all relative to VSMOW. [c]Percent mass loss calculated on samples during vacuum dehydroxylation. [d]$\delta^{18}O_{diatom}$ temperatures are calculated with the +94.4‰ value if available or corrected by adding the laboratory offset of +3.5‰, to adjust for the difference between equilibration using +94.4‰ rinse and laboratory DI rinse (−8.2‰). See appendix A for further information. [e]$\delta^{18}O_{diatom}$ temperatures use the linearized equations (3) and (4) presented in text. [f]$U^{k'}_{37}$ temperature data taken from Goni et al. (2001).

(<1 hr total time until samples were dry). Dried samples were stored in a vacuum desiccator. Sample purity was assessed using several independent methods, including X-ray diffraction, attenuated total reflection Fourier transform infrared spectroscopy and visual inspection via scanning electron microscopy prior to vacuum dehydroxylation and IRMS analysis via microfluorination (Menicucci et al., 2013; Menicucci et al., 2017). Only pure biogenic opaline samples exhibiting high quality, nondissolved diatom frustules were analyzed via microfluorination.

2.4. Sample Dehydroxylation and Microfluorination Analysis

Samples were dehydroxylated under vacuum prior to IRMS analysis in order to remove hydrous components (adsorbed and structural H_2O plus structural OH^-) from the covalently bound oxygen in the biogenic silica. Approximately 2 mg of each diatom sample was added to Ni capsules (Ni-201, no oxides), then loaded into a quartz tube connected to a vacuum manifold and slowly pumped down to <10 μTorr. Once under vacuum, samples were heated using a Carbolite HST 12/300 tube furnace with a Eurotherm 3216 controller. The heating cycle brought the sample temperature to 1060 °C within approximately 100 min, followed by an 8 hr (minimum) cooling cycle that allowed samples to return to ambient temperature. Sample mass was recorded before and after the vacuum dehydroxylation cycle to quantify mass loss. See Menicucci et al. (2017) for additional details.

Immediately following dehydroxylation, samples were loaded into Ag foil capsules that were preloaded with polytetrafluoroethylene (PTFE) (Chemours Zonyl® PTFE fluoroadditive type MP1200) and graphite (PTFE: graphite mass ratio of ~1625 μg:220 μg). Approximately 400 μg of diatom sample was loaded into each

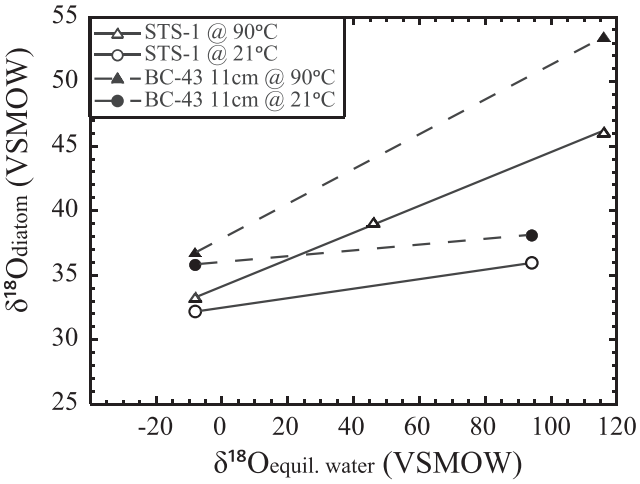

Figure 2. Experimental data for samples exposed to different $\delta^{18}O_{equil.\ water}$ solutions at 90 °C (data from Menicucci et al., 2017) and 21 °C. sediment trap sample, STS-1 (open symbols), and box core sample, BC-43 @ 11 cm (closed symbols), were equilibrated at 21 °C (circles, this study) and at 90 °C (triangles). Sample data values shift proportionally to the $\delta^{18}O_{equil.\ water}$ solutions used. Equilibration slopes for the samples are similar between the sediment trap (STS-1) and sediment core (BC-43, 11 cm) diatom samples, though sediment trap samples do show greater equilibration with the different $\delta^{18}O_{equil.\ water}$ solutions. Note that the slopes are lower in samples equilibrated at 21 °C than at 90 °C by an order of magnitude (~6 times smaller). Equilibration slopes and data from this plot can be found in Table 2.

capsule with the PTFE and graphite then gently stirred to homogenize the sample and additives. Sample capsules were then crimped and sealed for IRMS analysis.

Samples were analyzed using an Elementar vario PYROcube High Temperature Analyzer, connected to an Elementar VisION continuous flow IRMS. Excess halogens generated via PTFE pyrolysis were removed by substituting the typical quartz wool reactor packing with silver wool, and the addition of a series of inline traps. The traps, in order, were Sicapent (P_2O_5 with coloration), a 5 cm silver wool trap and a final magnesium perchlorate trap. In concert, these traps appear to remove residual free halogen reactive material.

Each analytical run on the PYROcube analyzed samples in groups of three, which included four replicates per sample. Each replicate was separated with a PTFE blank and each group of three samples were separated by standards. Measured $\delta^{18}O_{diatom}$ values within replicate sets across our analytical runs yield a precision range between ±0.0‰ and 0.4‰ (1σ standard deviation), with a mean precision of ±0.3‰ (1σ) for all samples. NBS-28 standard replicates scattered through each analytical run ($n = 29$) yielded a precision of ±0.1‰ (1σ). All $\delta^{18}O_{diatom}$ and $\delta^{18}O_{water}$ data in this study are reported relative to VSMOW.

2.5. Modern GB Water Column Hydrographic Data

October 1996 temperature and chlorophyll fluorescence data previously collected during the MOCE-5 cruise in the Gulf of California (Goni et al., 2001) were obtained from the Optical Oceanography Group, Oregon State University. Mean water column temperatures for the Gulf of California for October through December 1996 were obtained from the California Cooperative Oceanic Fisheries Investigations (CALCOFI) database (Robinson, 1973). These data are used in Figure 5.

3. Results

3.1. Equilibration Experiments

Average post vacuum dehydroxylation mass loss for the two STS-1 samples exposed to different $\delta^{18}O_{equil.\ water}$ solutions is 13.0% (Table 1). Mass loss for the BC-43 sediment samples (total mass loss per sample) varied between 9.2% and 11.2% with no discernible pattern between the shallowest and deepest BC-43 core samples. The sediment sample mass loss never exceeded the mass loss observed in the STS sediment trap samples.

Diatoms exposed to the two equilibration solutions at 21.2 °C produce a measurable offset in the $\delta^{18}O_{diatom}$ data (Figure 2). Values ranged between 32.2‰ and 35.9‰ in the STS-1 sediment trap sample, and from 35.8‰ to 38.1‰ in the 11 cm depth BC-43 sample (Table 1 and Figure 2) for $\delta^{18}O_{equil.\ water} = -8.2$‰ and +94.4‰, respectively. The slopes of equilibration lines between the $\delta^{18}O_{diatom}$ data from these two $\delta^{18}O_{equil.\ water}$ solutions are 0.036‰ / ‰ and 0.022‰ / ‰ (sample ‰ / equil. water ‰) for STS-1 and 11 cm depth BC-43 samples, respectively (Table 2).

Equilibration slopes obtained here at 21 °C (Table 1 and Figure 2) are approximately 4–5 times smaller than the slopes obtained on the same material at 90 °C in Menicucci et al., (2017). These results show rinse waters with different $\delta^{18}O_{equil.\ water}$ values produce quantifiable effects on $\delta^{18}O_{diatom}$ data across a range of temperatures used during standard laboratory cleaning and rinsing procedures. Equilibrating samples at lower laboratory temperatures reduces the magnitude of the exchange effect, thereby reducing the sensitivity of the $\delta^{18}O_{diatom}$ data to small differences among laboratory rinse water geochemistries.

3.2. GB $\delta^{18}O_{diatom}$ Record

Our sediment trap samples, including STS-1, cover a full annual cycle which begins at the start of the 1996 peak fall bloom, through August 1997. Overall mass loss for sediment trap samples only exposed to

Table 2
Equilibration Slope Data for Sediment Trap and Core Samples Showing Isotopic Alteration With Different Rinse Water Geochemistries at Ambient and Elevated Temperature

			Regression: $\delta^{18}O_{diatom} = a + b^a\delta^{18}O_{equil.\ water}$		
Sample	Sediment source	Date (CE)	*a*	*b*	*T* (°C)
STS-1	Planktonic	1996	32.5	0.036	21
BC-43, 11 cm	Sediment	1897	36.0	0.022	21
STS-1	Planktonic	1996	34.2 (±0.9)[a]	0.103 (±0.013)[a]	90
BC-43, 11 cm	Sediment	1897	37.9[a]	0.135[a]	90
UCD-DFS	Diatomite	—	32.5 (±1.4)[a]	−0.002 (±0.019)[a]	90

Note. *b* = slope is defined as $\delta^{18}O_{diatom}/\delta^{18}O_{equil.\ water}$. Equation errors are 95% confidence interval. Age model is from Goni et al. (2001).
[a]Data from Menicucci et al. (2017).

laboratory DI varied between 10.7% and 15.0%, and no correlation is observed between mass loss compared to sampling date or raw sample opal concentration. Values for $\delta^{18}O_{diatom}$ from these samples prepared with a $\delta^{18}O_{equil.\ water}$ solution of −8.2‰ range from 32.8‰ to 31.3‰, with the most positive values occurring during the winter (Table 1). Calculated temperatures (calculations explained in section 4.2 and Appendix A) for these $\delta^{18}O_{diatom}$ samples track closer to SST through most of the year, with the fall bloom samples yielding thermocline temperatures (Figure 3 and Table 1).

The upper 27 cm of box core BC-43 encapsulates roughly 220 years of upper water column hydrographic change in the GB. We observe a 1‰ down core increase in $\delta^{18}O_{diatom}$ between the upper two sediment intervals (~1979 and ~1966) followed by a further increase in $\delta^{18}O_{diatom}$ of 1.7‰ to the deepest group of samples from the late eighteenth century (Table 1 and Figure 4). This progressive $\delta^{18}O_{diatom}$ increase is disrupted for a brief period at the start of the twentieth century when we observe a ~1‰ decrease in values that lasts several decades. The full range of $\delta^{18}O_{diatom}$, +37.4‰ to 40.1‰, corresponds to a ~10 °C temperature decrease across the range of analyzed samples (see section 4 and Figure 4). Importantly, the $\delta^{18}O_{diatom}$ value obtained from our shallowest sediment interval (core collection year 1999; core top age ~1979) is ~1.5‰ more positive than the $\delta^{18}O_{diatom}$ value obtained from our sediment trap sample STS-1, which occurred during the peak fall bloom (Table 1).

4. Discussion

4.1. Exchangeable Oxygen Reactivity in Biogenic Opal

The equilibration experiments conducted here expand on earlier experiments conducted at 90 °C (Menicucci et al., 2017) and show that even when samples are held at ambient laboratory temperatures, both sediment trap and core samples yield different $\delta^{18}O_{diatom}$ values after exposure to isotopically distinct waters. However, the equilibration slopes at ~21 °C are 4–5 times smaller than slopes obtained for diatom samples exposed to equilibration waters at 90 °C (Figure 2) (Menicucci et al., 2017). The decrease in slopes at ~21 °C indicates the fraction of exchanged oxygen is substantially reduced at lower temperatures (Figure 2 and Table 2), although we are unsure if this is due to lower reaction rates or differences in exchangeability of some oxygen and lattice bound hydroxyl groups at lower temperature. Regardless, the influence of different rinse solutions on the final $\delta^{18}O_{diatom}$ values we obtain from IRMS analysis is reproducible and occurs on time scales commensurate with typical cleaning procedures (Crespin et al., 2008; Menicucci et al., 2017; Morley et al., 2004).

Assuming an initial 100% SiO_2 composition, we find 2.9% of oxygen in sediment trap (STS-1) diatoms is exchanged at ~21 °C, compared to 10.5% at 90 °C (Menicucci et al., 2017). Similarly, diatoms from BC-43, 11 cm depth, samples show 2.6% exchanged oxygen at ~21 °C, compared to 13.4% at 90 °C (Menicucci et al., 2017). These data substantiate previous research findings that oxygen exchange in biogenic opal is temperature dependent (Dodd et al., 2017; Labeyrie & Juillet, 1982; Webb & Longstaffe, 2000), and provide evidence that oxygen isotopic equilibration between frustules and rinse water geochemistry is occurring in the laboratory during sample preparation. Importantly, our data show that the exchange of rinse water oxygen

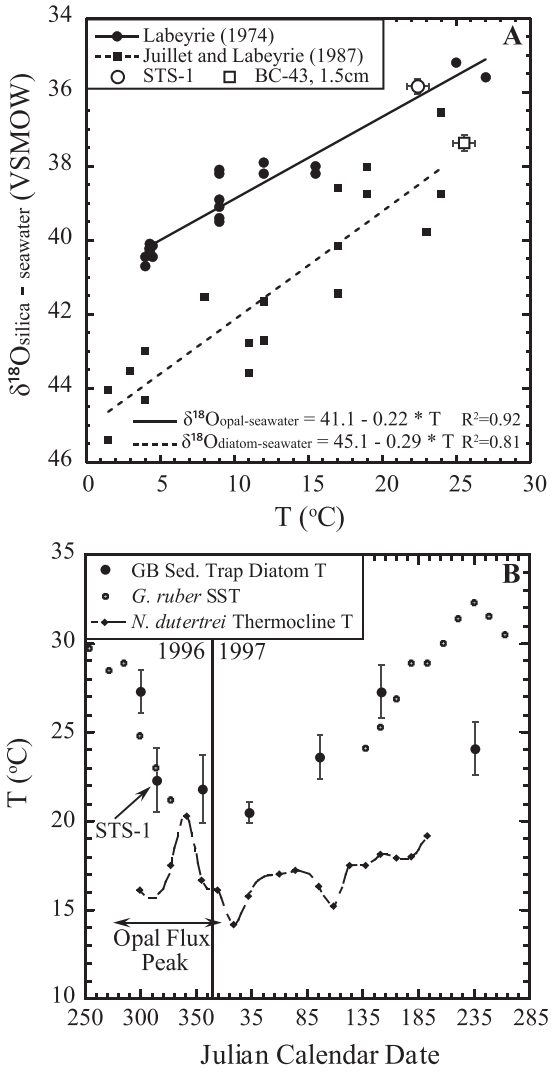

Figure 3. (a) $\delta^{18}O_{biogenic\ silica\text{-}water}$ data from Labeyrie (1974) (closed circles) and Juillet-Leclerc and Labeyrie (1987) (closed squares), plotted against temperature (°C). Sediment trap sample STS-1 (open circle) and box core sample, BC-43, 1.5 cm depth, (open square) $\delta^{18}O_{diatom}$ data from this study are also included. These latter samples were equilibrated in the laboratory at 21 °C in a $\delta^{18}O_{equil.\ water}$ solution of +94.4‰ (VSMOW). Linear relationships generated through the Labeyrie (1974) $\delta^{18}O_{opal}$ data from silica samples derived from different living organisms and Juillet-Leclerc and Labeyrie (1987) data from fossil core top $\delta^{18}O_{diatom}$ samples yield relationships that can be used to compute temperatures for either living or fossil diatom data. (b) Sediment trap samples collected between 1996 and 1997, covering the peak fall diatom bloom and including samples from low opal flux times in the winter and summer. Except for STS-1, these samples were rinsed only with our laboratory DI water, and an offset correction of +3.5‰ was added to the raw $\delta^{18}O_{diatom}$ data (Table 1) to bring them back onto the empirical Labeyrie (1974) (equation (3)). STS-1's computed temperature using the value measured after exchange with the +94.4‰ $\delta^{18}O_{equil.\ water}$ solution is highlighted. $\delta^{18}O_{foram}$ temperatures using *G. ruber* for SST and *N. dutertrei* for the lower thermocline taken from Wejnert et al. (2010). Note that $\delta^{18}O_{diatom}$ temperatures occur between the cooler thermocline base and the warmer SST during peak fall bloom, trending cooler as the fall bloom extends into December. Laboratory DI offset correction details available in appendix a. Error bars are ±1σ standard error for $\delta^{18}O$ data and 1σ standard deviation for temperature conversion.

with fully coordinated lattice bound oxygen sources is predictable and reproducible across a range of preparation temperatures commonly used in many different laboratories. However, the isotopic composition of the data are constrained by the original tetrahedrally bound oxygen $\delta^{18}O$ value within the biogenic opal lattice. This supports the foundational premise that environmental signals remain preserved in diatom frustule oxygen isotopes after incorporation into the sediment, and importantly, also after laboratory preparation.

4.2. Revising a Temperature-$\delta^{18}O_{biogenic\ silica}$ Relationship

The first empirical temperature versus $\delta^{18}O_{biogenic\ silica}$ calibration was generated by Labeyrie (1974) on a suite of "newly deposited" diatoms and living siliceous sponge spicules collected from marine sources across a temperature range between 4 and 27 °C. This "$\delta^{18}O_{opal}$" to temperature calibration utilized data from samples that were obtained using a version of the fluorination method detailed by Clayton and Mayeda (1963). This yielded the relationship:

$$T = 5 - 4.1 * \left(\delta^{18}O_{opal} - \delta^{18}O_{seawater} - 40\right) \quad (1)$$

where all $\delta^{18}O$ values were presented relative to SMOW. Here the authors arbitrarily subtracted 40‰ from the measured $\delta^{18}O_{opal}$ values in order to more easily compare opal data with $\delta^{18}O$ values being produced for calcite on the PDB scale. Later, Leclerc and Labeyrie (1987) generated a core top $\delta^{18}O$ to temperature calibration using an interhemispheric transect of cores between 54°N and 54°S, using exclusively fossil diatoms from sediment core tops which grew between 1.5 and 24 °C, which they called "$\delta^{18}O_{diatom}$" versus temperature. Again, 40‰ was subtracted from the relationship as explained above:

$$T = 17.2 - 2.4 * \left(\delta^{18}O_{diatom} - \delta^{18}O_{seawater} - 40\right) - 0.2 * \left(\delta^{18}O_{diatom} - \delta^{18}O_{seawater} - 40\right)^2 \quad (2)$$

These relationships display a clear offset from each other (Figure 3a).

Studies of $\delta^{18}O_{diatom}$ from fresh water environments have shown that the tetrahedrally bound oxygen in diatoms undergoes as much as a 7‰ enrichment in ^{18}O after frustules are deposited in the sediment (Dodd et al., 2012). Similar enrichments have been observed in marine sediment diatoms, yielding values that range from 2.4‰ to 10.1‰ higher than diatoms from nearby sediment trap samples (Schmidt et al., 2001). This enrichment indicates that the diatom frustules experience a rapid geochemical transformation after sedimentation, while still retaining their near surface environmental signal (Dodd et al., 2012; Schmidt et al., 2001). This enrichment could be due to post sedimentation diagenesis related to the natural loss of structural hydroxyl in the biogenic opal (Dodd et al., 2012; Dodd et al., 2017; Menicucci et al., 2017) or some other as yet unidentified mechanism.

The enrichment in $\delta^{18}O_{diatom}$ that occurs once the frustules are incorporated into the sediment does not appear to compromise the original temperature signal carried by the biogenic opal oxygen within the silicate lattice. This can be seen in the offset between equations (1) and (2). In Figure 3a, we replot the published data of Labeyrie (1974) and Leclerc and Labeyrie (1987) after eliminating the 40‰ constant offset that was

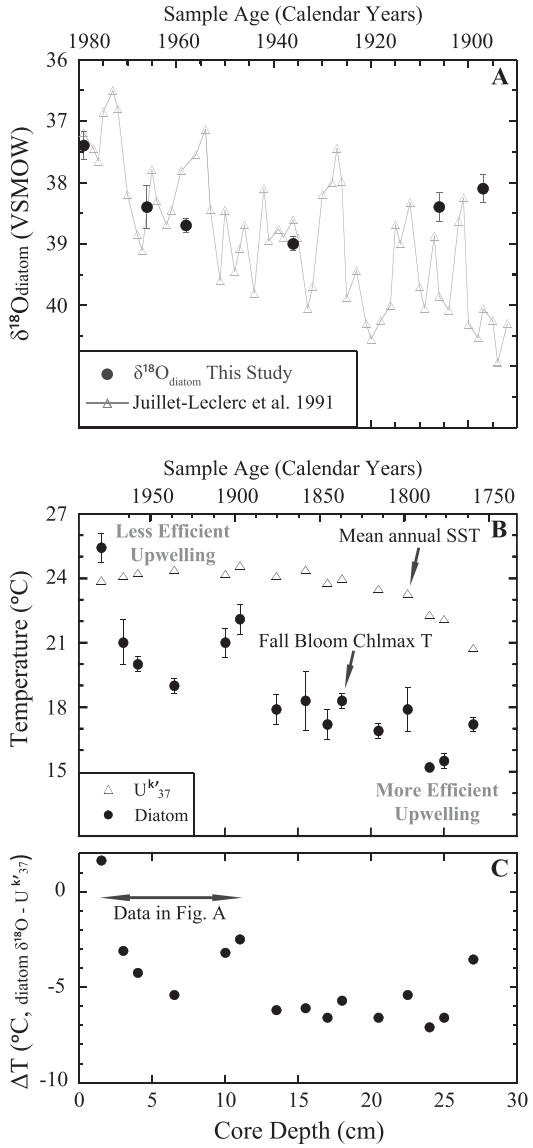

Figure 4. $\delta^{18}O_{diatom}$ data from this study plotted against existing data sets. (a) Sediment samples analyzed by Juillet-Leclerc et al. (1991) from a nearby Guaymas Basin site using controlled isotope exchange fluorination line techniques (open triangles), plotted with the upper six samples in BC-43 that correspond to the same time period (closed circles). Note the excellent agreement in $\delta^{18}O_{diatom}$ values among these overlapping samples. (b) Comparison of BC-43 $U^{k'}_{37}$ SST data (triangles) presented by Goni et al. (2001) and $\delta^{18}O_{diatom}$ temperature data from this study, showing distinct temperature profiles for the SST and the Chl_{max} (circles, this study). Data converge in the most recent sampling data, suggesting reduced upwelling efficiency due to a deeper thermocline in modern times. We interpret upwelling as being more efficient historically. (c) the calculated difference between sample $U^{k'}_{37}$ SST and the calculated $\delta^{18}O_{diatom}$ Chl_{max} temperature in core BC-43, illustrating how much warmer the Chl_{max} has become over time, even when SST was relatively steady, suggesting a deeper thermocline in modern times with stronger summer stratification. Temperatures derived from BC-43 $\delta^{18}O_{diatom}$ data use equation (4) and are plotted after equilibration with +94.4‰ $\delta^{18}O_{equil.\ water}$ solution to bring samples onto the empirical temperature calibration (for further details, see section 4.2). Error bars on the BC-43 data are ±1σ standard error measured for each sample.

inserted into the original equations. The resulting linearized regressions through their data yield:

$$T = \left(41.1\ [\pm 0.54] - \delta^{18}O_{opal-seawater}\right)/0.22\ [\pm 0.05] \quad (3)$$

and

$$T = \left(45.1\ [\pm 1.57] - \delta^{18}O_{diatom-seawater}\right)/0.29\ [\pm 0.11] \quad (4)$$

for the two data sets, respectively. All values in these recalculated equations are relative to SMOW. We utilize equations (3) and (4) to evaluate the sediment trap and sediment core $\delta^{18}O_{diatom}$ data collected in this study, respectively, because the relationships were generated on material that was similar to that analyzed here. At the 95% confidence level, the slopes of equations (3) and (4) are indistinguishable but are offset by an average of 3.7‰ across the range of calibrated temperatures. This offset is within the range of post depositional ^{18}O-enrichment after final sedimentation discussed earlier (Dodd et al., 2012; Dodd et al., 2017; Schmidt et al., 2001) and observed when $\delta^{18}O_{diatom}$ data from STS-1 and the 1.5 cm interval from BC-43, are plotted with data in equations (3) and (4), respectively (Figure 3a).

4.3. Converting Microfluorination $\delta^{18}O_{diatom}$ Data to Temperature in the GB

In order to use equations (3) and (4) to calculate temperature from the $\delta^{18}O_{diatom}$ data generated we need to compensate for the offset between the samples we measured after rinsing with UC Davis laboratory DI water ($\delta^{18}O_{equil.\ water} = -8.2$‰) and the data in these empirical calibrations. To calculate this offset, we use a measured GB $\delta^{18}O_{seawater}$ value of −0.3‰ and assume the diatoms grew within the Chl_{max} during the fall bloom. Sample STS-1 was collected during the early fall bloom when the Chl_{max} had a mean temperature of 24 °C (22–26 °C across the Chl_{max} depth range) (Thunell, 1998; Thunell et al., 1993; Thunell et al., 1996). However, there is some evidence that diatoms living lower in the Chl_{max} are more densely silicified (Taylor, 1985), and thus may contribute a greater mass proportion to the sediment trap. Therefore, we select a slightly cooler growth temperature for STS-1, 23 °C, to reflect deeper Chl_{max}, conditions.

The computed equilibration slopes from our STS-1 sample at 21 °C (Figure 2 and Table 2) demonstrate that a large continuum of $\delta^{18}O_{diatom}$ values can be measured depending on the $\delta^{18}O_{equil.\ water}$. Based on the above estimate for the STS-1 temperature, equation (3) predicts that STS-1 should have a $\delta^{18}O_{diatom}$ value of 35.8‰. This value was determined by inverting the 21 °C equilibration slope relationship for STS-1 (Table 2):

$$\delta^{18}O_{target\ eq.water} = \left(\delta^{18}O_{predicted\ diatom} - 32.5\right)/0.036 \quad (5)$$

This $\delta^{18}O$ value is within 0.1‰ of the value we measured for STS-1 using a $\delta^{18}O_{equil\ water}$ of +94.4‰ (Table 1) and yields a temperature for the STS-1 sample of 22.3 °C. Had we prepared STS-1 with a $\delta^{18}O_{equil.\ water}$ value of 91.7‰, we would have produced the exact $\delta^{18}O_{diatom}$ value predicted by equation (3) at 23 °C. The 0.1‰ difference is well within the

precision of the microfluorination technique measurements so we do not adjust the diatom values for the $\delta^{18}O_{equil.\ water}$ value, 94.4‰, we used during sample preparation.

Previous work in the GB on thermocline dwelling planktonic foraminifera from the STS site offers insight into our $\delta^{18}O_{diatom}$ data and the application of equation (4) to generate Chl_{max} temperatures using a $\delta^{18}O_{equil.\ water}$ value of 94.4‰ when processing fossil material. Analyses of the nonspinose species, *Neogloboquadrina dutertrei* and *Globorotalia menardii*, demonstrate these species accurately record the annual range of thermocline temperatures from late summer through fall and winter seasons in the GB (Davis et al., 2019) (Wejnert et al., 2010), with *N. dutertrei* occupying a slightly shallower habitat depth than *G. menardii* (Spero et al., 2003) (Wejnert et al., 2010). Oxygen isotope data collected on these species between 1991 and 1997 yield average summer temperatures immediately prior to upwelling of 23.7 and 25.4 °C, respectively (Wejnert et al., 2010). Average winter temperatures for the two species show that thermocline temperatures range between 17.8 and 18.3 °C (Wejnert et al., 2010). These temperatures bracket the range that the diatoms encounter between the initiation of the fall bloom (average summer temperatures) and winter thermocline temperatures after upwelling ceases in December the thermocline, resulting in an isothermal mixed layer (Davis et al., 2019; Wejnert et al., 2010).

Based on the fall-weighted diatom flux history of the GB (Thunell, 1998), BC-43 sediment samples are most likely dominated by diatoms that grew predominantly within the Chl_{max} during the fall bloom prior to winter conditions. The background opal flux prior to the 1996 fall diatom bloom ranges from 0.059 to 0.178 $g{\cdot}m^{-2}{\cdot}day^{-1}$ (Thunell, 1998). However, during the 1996 diatom bloom opal flux reached as high as 0.668 $g{\cdot}m^{-2}{\cdot}day^{-1}$, and sustained fall bloom opal export has been measured consistently as 3–4 times as high as background levels through the end of December (Thunell, 1998; Thunell et al., 1994). Background opal flux levels typically resume by the end of January (Thunell, 1998; Wejnert et al., 2010). We therefore consider the range of temperatures recorded by *N. dutertrei* and *G. menardii* as depth and seasonal constraints for the $\delta^{18}O_{diatom}$ data, ranging from 23 to 26 °C during the bloom initiation to 17 to 18 °C at the end of the bloom. The temperature we obtain from the STS-1 $\delta^{18}O_{diatom}$ data using equation (3), 22.3 °C, is within the range of these foraminifera-based thermocline temperatures, and is bracketed by the warmer SST recorded by *Globigerinoides ruber* (Figure 3b).

The BC-43, 1.5 cm core top diatom material represents a seasonally weighted sample that is likely dominated by the fall flux. Here, we must use equation (4) to interpret the BC-43, 1.5 cm $\delta^{18}O_{diatom}$ value of 37.4‰ (Figure 4 and Table 1) because the core samples have already undergone the water column to sediment $\delta^{18}O$ transformation described above. The BC-43, 1.5 cm $\delta^{18}O_{diatom}$ data yields a temperature of 25.5 °C which is on the warm end of the thermocline temperature range from the nonspinose foraminifera, but within the expected range (Davis et al., 2019; Wejnert et al., 2010).

Although the BC-43, 1.5 cm $\delta^{18}O_{diatom}$ data yield warmer Chl_{max} temperatures than we compute for the STS-1 sediment trap sample, we note that BC-43, 1.5 cm from ~1979 contains one (or more) complete years of sedimented diatoms that were deposited during an El Niño year (Davis et al., 2019). In contrast, STS-1 is part of an annual sequence that starts with a fall bloom during a La Niña year, raising the possibility that the temperature differences we observe between STS-1 and BC-43, 1.5 cm reflect seasonal versus annual integrations and El Niño–Southern Oscillation variability. Nevertheless, both reconstructed temperatures fall within the range of modern Chl_{max} temperatures for the region and are in agreement with modern $\delta^{18}O_{foram}$ temperature data (Davis et al., 2019; Wejnert et al., 2010).

The signal shown in our cumulative sediment trap samples captures a distinct annual cycle of diatom productivity in the GB (Figure 3b). This annual diatom temperature signal closely tracks the significant increase in opal export to the sediment during peak productivity, with the peak opal flux temperatures falling between SSTs recorded by *G. ruber* and lower thermocline temperatures recorded by *N. dutertrei* (Figure 3b). During nonbloom times of winter and spring, the $\delta^{18}O_{diatom}$ temperatures appear to track more closely with mixed layer SST signals preserved by *G. ruber*, including an early warming in June of 1997, an El Niño year (Thunell et al., 1999) and then record a cooler signal that again falls between the lower thermocline and warmer SSTs (Figure 3b).

Our reconstructions of temperature from the 1996–1997 sediment trap data lend further insight into the annual dynamics influencing the sedimentary signal preserved in the $\delta^{18}O_{diatom}$ data. Temperature

conversions for the sediment trap $\delta^{18}O_{diatom}$ data were done using the laboratory DI offset equation in Appendix A (equation (A1)), because these samples were not secondarily equilibrated with any $\delta^{18}O_{equil.\ water}$ solutions, and instead were rinsed only with our laboratory DI. Details on how this offset is calculated, and the potential implications of diatom opal maturation on calculations for thermocline temperatures moving down core are described in Appendix A. For our laboratory, when 3.5‰ is added to our measured STS $\delta^{18}O_{diatom}$ data (Table 1) we can use equation (3) to calculate temperature. The temperatures we calculate in the annual sediment trap record fit well with diatom biology during bloom and nonbloom seasonality, despite the limitation of only 1 year of data. Visual inspection of diatoms from the sediment trap show a prevalence of large centric diatoms from the genus *Coscinodiscus* spp., among others. While we did not conduct point count analyses to determine floral species abundances and fluctuations over time, other authors have regularly monitored algal floral variation nearby (Sancetta, 1995; Thunell et al., 1996). These studies show that while the dominant species in the GB are generally persistent, there are distinct seasonal patterns in the secondary taxa (Sancetta, 1995), which may live in different parts of the euphotic zone and thus integrate a slightly different signal into the sediment traps during sampling. Diatom species are known to have irradiance preferences, which have been documented in the Gulf of California (Verdugo-Diaz et al., 2012; Verdugo-Diaz & Garate-Lizarraga, 2018), and which would also be balanced by species thermal preferences for growth. Combined, these factors directly lead to vertical species partitioning during nonbloom times, with such signals being homogenized during the mixing of assemblages in the sediment trap. During peak opal flux in the fall, the $\delta^{18}O_{diatom}$ temperatures fall between the $\delta^{18}O_{foram}$ SST (*G. ruber*) and lower thermocline (*N. dutertrei*) temperatures (Figure 3b), and this mid-depth signal is most likely representative of the Chl_{max}. During nonpeak opal flux, it is likely a slightly different assemblage occupies a larger area in the euphotic zone. This persists until summer warming begins to stratify the water column and the diatom assemblage again shifts to one with a habitat preference that is deeper, and within the Chl_{max} (Figure 3b). This biological information, in concert with the constraints of the $\delta^{18}O_{foram}$ temperature data, strongly suggest our sediment core samples are strongly weighted toward recording fall bloom activity.

4.4. GB Water Temperature Reconstructions

The first GB $\delta^{18}O_{diatom}$ sedimentary record was a high resolution effort that spanned most of the twentieth century (Figure 4a) (Juillet-Leclerc et al., 1991; Juillet-Leclerc & Schrader, 1987). These data were generated using classical fluorination methods. The authors concluded that the $\delta^{18}O_{diatom}$ data recorded a SST increase of approximately 6 °C between 1890 and 1980, possibly due to a decrease in wind-driven upwelling. Particularly relevant for our study is that the uppermost six diatom samples analyzed from boxcore BC-43 overlap with the samples in the Juillet-Leclerc et al. (Juillet-Leclerc et al., 1991) record. Figure 4 displays the two $\delta^{18}O_{diatom}$ data sets on a common age scale as similarly utilized by Goni et al. (2001) using ^{210}Pb excess (Pride, 1997) and Juillet-Leclerc et al. (1991) using a combination of ^{137}Cs and varve counting. Age model offsets cannot be estimated but are likely subdecadal, although Juillet-Leclerc et al. (1991) did report varve disruption in a part of their record. The two data sets display data that are indistinguishable and show similar $\delta^{18}O_{diatom}$ variability and ranges notwithstanding the differences in preparation technique for the two sample sets. We also see the progressive late twentieth century Chl_{max} warming in the high resolution record that culminates in our 25.5 °C estimate for the BC-43, 1.5 cm sample discussed above. We consider this strong support that data generated using the preparation and analysis techniques employed in this study are directly comparable to the more classic fluorination methodologies used in the past.

Using equation (4) to interpret the BC-43 $\delta^{18}O_{diatom}$ data shows that GB Chl_{max} temperatures range between 15.2 and 25.5 °C (Figure 4b) during the past 220 years, The period between ~1870 CE and the late eighteenth century suggests a cooler GB thermocline (relative to the twentieth century) that ranged between ~15 and 18 °C. These results can be compared directly to published alkenone $U^{k'}_{37}$ temperatures from BC-43 (Goni et al., 2001; Goni et al., 2006) which show that the thermocline was ~5–7 °C cooler than mean annual SST during this time interval (Figure 4b). This offset is due to a combination of the maximum flux of alkenones occurring during the summer before the peak opal flux of the fall diatom bloom (Goni et al., 2001), and that alkenones yield mean annual SST versus thermocline temperatures in the Chl_{max} by the diatoms (Goni et al., 2001; Goni et al., 2006). Overall, both $\delta^{18}O_{diatom}$ based temperatures and $U^{k'}_{37}$ SSTs show cool historical GB temperatures (Figure 4b) during this period.

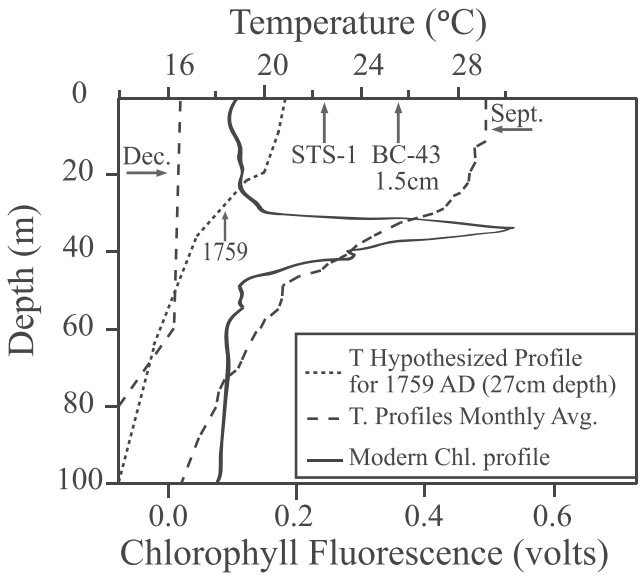

Figure 5. Water column temperature and chlorophyll fluorescence for the upper 100 m of the GB and hypothesized temperature profile for 1759 CE, based on $\delta^{18}O_{diatom}$ and $U^{k'}_{37}$ data. Point data for $\delta^{18}O_{diatom}$ from STS-1 and BC-43, 1.5 cm samples are noted with single arrows pointing to their respective temperatures. This figure shows measured water temperatures during the start and end of the fall diatom bloom in the GB using September and December temperature data (dashed lines) over the upper 100 m; measured monthly temperatures are composite averages from Robinson (1973) and re-illustrated in Wejnert et al. (2010). The location of the Chl_{max}, where $\delta^{18}O_{diatom}$ temperatures are recorded, is shown in the peak of the chlorophyll fluorescence data (solid line), taken from Goni et al. (2001) (collected in 1999, MOCE-5 cruise). The fine dotted line shows our hypothesized fall bloom profile temperature profile for 1759 (core BC-43, 27 cm core depth). This hypothesized temperature reconstruction is constrained by the SST data ($U^{k'}_{37}$, 20.7 °C) and Chl_{max} data ($\delta^{18}O_{diatom}$, 17.2 °C) from this 27 cm interval. This hypothesized thermocline shape is modeled off the transition from warm to isothermal which occurs in the diatom bloom (September to December). The 1759 thermocline must have been cooler, and most likely shallower, due to cooler SST and much cooler upper thermocline T.

The diatom data record a considerably warmer thermocline during the second half of the twentieth century with Chl_{max} temperatures between 19 and 25.5 °C. The $\delta^{18}O_{diatom}$ data appear to document a rapid warming followed by a brief period of cooling of the Chl_{max} during the early/mid twentieth century (Figure 4b). However, the higher resolution Juillet-Leclerc et al. (Juillet-Leclerc et al., 1991) diatom record (Figure 4a) shows that the range of our $\delta^{18}O_{diatom}$ values falls well within the decadal scale variability of GB thermocline temperatures that are likely due to El Niño–Southern Oscillation variability in the region, rather than a prolonged multi-decadal period of cooling. Nevertheless, both data sets agree with other observations that the GB thermocline has undergone a gradual warming that began in the twentieth century or before (Goni et al., 2001; Goni et al., 2006). The core-top BC-43, 1.5 cm temperature we obtain suggests that late twentieth century Chl_{max} temperatures during the fall bloom are comparable to mean annual SST for the GB (Figures 3b and 4).

Juillet-Leclerc et al. (1991) argued that colder $\delta^{18}O_{diatom}$ temperatures during the early twentieth century suggest upwelled waters were derived from deeper sources than the modern water column, which would indicate more efficient upwelling. Goni et al. (2006) further argued that in the last 50 years, upwelling was more intense in the GB than in the prior half century, attributing warmer SSTs to slight changes in insolation. However, our data suggest the Chl_{max} temperatures have increased this century whereas the mean annual SST remained relatively unchanged. We therefore suggest the $\delta^{18}O_{diatom}$ data are not a measure of upwelling intensity, but rather a qualitative measure of upwelling efficiency in the GB.

The fall shoaling of the thermocline in the GB is influenced by the southward migration of the western North American subtropical high and the Intertropical Convergence Zone (Cheshire et al., 2005). As these atmospheric systems shift southward, winds out of the NW strengthen, initiating GB upwelling (Goni et al., 2006; Juillet-Leclerc et al., 1991; Juillet-Leclerc & Schrader, 1987). We hypothesize that since the late nineteenth century, upwelling has become less efficient with summer thermal stratification extending later into

the fall. Together this has produced a deeper mixed layer/thermocline boundary prior to the initiation of upwelling (Figure 5) (Juillet-Leclerc et al., 1991; Juillet-Leclerc & Schrader, 1987). During the nineteenth century, lower initial SST may have been associated with a shallower thermocline depth, thereby allowing upwelling to more rapidly and efficiently break down the thermal stratification, allowing the diatoms to bloom in cooler Chl_{max} thermocline waters (Figure 5). Goni et al. (2006) speculated that a northward shift in the position of the subtropical high may contribute to a delayed onset of fall-winter upwelling in the GB. During the past half century, $\delta^{18}O_{diatom}$ temperatures have approached those equivalent to mean annual alkenone SST (Figure 4). This suggests summer warmth is now extending into the fall diatom bloom at Chl_{max} depths and that effective mixing of cooler upwelling waters into this larger pool of warm surface waters has become less efficient in the early fall (Figure 5).

5. Summary

Measurement of $\delta^{18}O_{diatom}$ has potential for alteration under laboratory conditions. We present data showing that diatom biogenic silica exchanges with surrounding water at ambient room temperature (21 °C) and on time scales commensurate with typical laboratory cleaning procedures. Our data demonstrate that the exchange between $\delta^{18}O_{equil.\ water}$ solutions results in predictable changes in $\delta^{18}O_{diatom}$ at ~21 °C. We utilized a sample pretreatment that includes a final rinse/equilibration of the biogenic opal with an enriched $\delta^{18}O_{equil.\ water}$ solution prior to dehydroxylation. This final rinse brings the $\delta^{18}O_{diatom}$ values onto previously published empirical relationships between $\delta^{18}O_{diatom}$ and temperature, which were also recalculated based on the original data sets.

Using our sample pretreatment, empirical $\delta^{18}O_{diatom}$ to temperature conversions allowed a comparison of upper water column temperature data to existing temperature proxies. We demonstrated our $\delta^{18}O_{diatom}$ temperature data are in agreement with modern $\delta^{18}O_{foram}$ temperatures. A data set containing an annual cycle of sediment trap samples from 1996 to 1997 shows good agreement between the $\delta^{18}O_{diatom}$ and $\delta^{18}O_{foram}$ calculated temperatures and suggests the sedimentary record in the GB is heavily biased to record the fall diatom bloom. Comparison of our sediment core $\delta^{18}O_{diatom}$ data to previously published $\delta^{18}O_{diatom}$, and $U^{k'}_{37}$ SST data from core BC-43 show that our $\delta^{18}O_{diatom}$ measurements have similar ranges and reflect similar trends toward more negative $\delta^{18}O_{diatom}$ values in the modern water column. We suggest that the sedimentary record of $\delta^{18}O_{diatom}$ temperatures are reflective of fall bloom chlorophyll maximum. temperatures and can be paired effectively with the annual SSTs recorded by $U^{k'}_{37}$. Our interpretation of the $\delta^{18}O_{diatom}$ data suggests a progressive decrease in upwelling efficiency moving forward in time to the modern water column. We hypothesize that historical water column conditions in the GB included more efficient upwelling due to a historically shallower thermocline in the mixed layer and that the modern mixed layer has become more strongly stratified with a deeper thermocline as a result of more intense summer heating since 1759 CE

Appendix A: Laboratory Offset Corrections for Paleoceanographic Applications

We used a final rinse that is enriched in ^{18}O on sample STS-1 and the BC-43 sediment core samples in this study in order to yield $\delta^{18}O_{diatom}$ data that can be interpreted with equations (3) and (4). Data show similar enrichments of BC-43 sediment and STS-1 samples when using a single enriched $\delta^{18}O_{equil.\ water}$ solution (Figure 2a), with the single solution bringing both sediment trap and sediment core samples onto the empirical temperature equations. There are also similar slopes for equations (3) and (4), despite the different source material. This suggests that one can utilize a single $\delta^{18}O_{target\ eq.\ water}$ (synonymous with a laboratory's local rinse water) for equilibration and that the values obtained can be offset corrected so that the measured $\delta^{18}O_{diatom}$ data can be directly interpreted with the empirical calibrations of equations (3) and (4).

In order to calculate an empirical offset correction for $\delta^{18}O_{diatom}$ data that are generated from samples rinsed with a laboratory's DI such that the $\delta^{18}O_{diatom}$ data can be interpreted using equations (3) and (4), it is necessary to know the rinse solution water $\delta^{18}O$ value and calculate an offset correction to adjust the data as if samples were equilibrated with the $\delta^{18}O_{equil.\ water}$ solution of +94.4‰ used in experiments for this study. If we rearrange equations (3) and (5) so the predicted $\delta^{18}O_{diatom}$ measurement (based on a known temperature) is an isolated variable, and then set these two equations equal to each other by equating $\delta^{18}O_{predicted\ diatom}$ and $\delta^{18}O_{opal\ -\ seawater}$, we obtain a simple relationship that computes the

‰ difference between raw microfluorination $\delta^{18}O_{diatom}$ measurements and the empirical temperature calibration of equation (3):

$$\delta^{18}O_{diatom}\ \text{Offset} = -8.6 + 0.036 * \delta^{18}O_{\text{lab DI rinse water}} - \delta^{18}O_{seawater} + 0.22 * T_{seawater} \quad \text{(A1)}$$

The $\delta^{18}O$ offset for sediment trap samples using our laboratory DI water (−8.2‰) is −3.5‰. A similar rearrangement can be done with equation (4) in order to calculate an offset for sediment core samples:

$$\delta^{18}O_{diatom}\ \text{Offset} = -9.1 + 0.022 * \delta^{18}O_{\text{lab DI rinse water}} - \delta^{18}O_{seawater} + 0.29 * T_{seawater} \quad \text{(A2)}$$

The $\delta^{18}O$ offset for sediment core samples with our laboratory DI water is −2.1‰. These offsets can be corrected by adding the inverse, +3.5‰ or +2.1‰, to the sediment trap or sediment core $\delta^{18}O_{diatom}$ data, respectively, that have been cleaned and rinsed with laboratory DI. This correction thus brings the samples onto the empirical calibrations of equations (3) and (4).

We applied this +3.5‰ correction to the sediment trap samples which were prepared using only DI water (the STS-1 sample was prepared twice, having been rinsed in both DI and our enriched ^{18}O water). Temperatures were calculated using the offset corrected $\delta^{18}O_{diatom}$ values, and applying equation (3) (Table 1). These results demonstrate the applicability of this simple correction for modern samples and demonstrate the utility of this method for interpreting $\delta^{18}O_{diatom}$ data in a paleoceanographic context. Future use of the correction calculated in equation (A2) moving down core would inherently be limited to recent time frames where the diatoms demonstrate similar exchangeability and have not undergone substantial sediment maturation (Dodd et al., 2017; Menicucci et al., 2017).

Acknowledgments
We thank M. Goni for generously providing his GB, BC-43 sediment core samples for this project. Funding was provided by the National Science Foundation to H. J. S. (Award 1334686), and a Bodega Marine Laboratory Graduate Student Fellowship to A. J. M. We thank L. Beaudin, D. Caro, and E. Schick for their assistance with sample cleaning and preparation. Water isotope analyses were performed by E. Delgado in the Stable Isotope Facility (SIF), UC Davis. We thank R. E. M. Rickaby and J. J. Tyler for sharing their unpublished data. Valuable feedback was provided by J. Fehrenbacher and O. Branson, in addition to the reviewers of this manuscript prior to publication. We also thank J. Matthews and her staff at the UC Davis SIF for their continued support and valuable feedback during the development of the microfluorination technique and its applications. All data used for this publication are available in Table 1 and are archived in the PANGAEA database (https://doi.org/10.1594/PANGAEA.905179). During the research phase of this project, our friend, colleague, and mentor, Bob Thunell, passed away. This project builds on Bob's passion to understand the linkage between the geochemistry of living planktonic organisms and the paleoceanographic record they leave behind in the sediment column. Bob's insight, generosity, and collaborations will be sorely missed.

References

Brandriss, M. E., O'Neil, J. R., Edlund, M. B., & Stoermer, E. F. (1998). Oxygen isotope fractionation between diatomaceous silica and water. *Geochimica et Cosmochimica Acta*, *62*(7), 1119–1125. https://doi.org/10.1016/s0016-7037(98)00054-4

Cheshire, H., Thurow, J., & Nederbragt, A. J. (2005). Late Quaternary climate change record from two long sediment cores from Guaymas Basin, Gulf of California. *Journal of Quaternary Science*, *20*(5), 457–469. https://doi.org/10.1002/jqs.944

Clayton, R. N., & Mayeda, T. K. (1963). The use of bromine pentafluoride in the extraction of oxygen from oxides and silicates for isotopic analysis. *Geochimica et Cosmochimica Acta*, *27*(JAN), 43–52. https://doi.org/10.1016/0016-7037(63)90071-1

Clayton, R. N., Mayeda, T. K., & Oneil, J. R. (1972). Oxygen isotope-exchange between quartz and water. *Journal of Geophysical Research*, *77*(17), 3057–3067. https://doi.org/10.1029/JB077i017p03057

Crespin, J., Alexandre, A., Sylvestre, F., Sonzogni, C., Pailles, C., & Garreta, V. (2008). IR laser extraction technique applied to oxygen isotope analysis of small biogenic silica samples. *Analytical Chemistry*, *80*(7), 2372–2378. https://doi.org/10.1021/ac071475c

Crespin, J., Sylvestre, F., Alexandre, A., Sonzogni, C., Pailles, C., & Perga, M. E. (2010). Re-examination of the temperature-dependent relationship between delta O-18(diatoms) and delta O-18(lake water) and implications for paleoclimate inferences. *Journal of Paleolimnology*, *44*(2), 547–557. https://doi.org/10.1007/s10933-010-9436-2

Davis, C. V., Fuqua, L., Pride, C., & Thunell, R. (2019). Seasonal and interannual changes in planktic foraminiferal fluxes and species composition in Guaymas Basin, Gulf of California. *Marine Micropaleontology*, *149*, 75–88. https://doi.org/10.1016/j.marmicro.2019.05.001

DeMaster, D. J., and H. D. H. K. Turekian (2003), 7.04—The diagenesis of biogenic silica: Chemical transformations occurring in the water column, seabed, and crust, in *Treatise on Geochemistry, Edited*, pp. 87-98, Pergamon, Oxford.

Dodd, J. P., & Sharp, Z. D. (2010). A laser fluorination method for oxygen isotope analysis of biogenic silica and a new oxygen isotope calibration of modern diatoms in freshwater environments. *Geochimica et Cosmochimica Acta*, *74*(4), 1381–1390. https://doi.org/10.1016/j.gca.2009.11.023

Dodd, J. P., Sharp, Z. D., Fawcett, P. J., Brearley, A. J., & McCubbin, F. M. (2012). Rapid post-mortem maturation of diatom silica oxygen isotope values. *Geochemistry, Geophysics, Geosystems*, *13*(9), 1–12. https://doi.org/10.1029/2011gc004019

Dodd, J. P., Wiedenheft, W., & Schwartz, J. M. (2017). Dehydroxylation and diagenetic variations in diatom oxygen isotope values. *Geochimica et Cosmochimica Acta*, *199*, 185–195. https://doi.org/10.1016/j.gca.2016.11.034

Goni, M. A., Hartz, D. M., Thunell, R. C., & Tappa, E. (2001). Oceanographic considerations for the application of the alkenone-based paleotemperature U-37(K′) index in the Gulf of California. *Geochimica et Cosmochimica Acta*, *65*(4), 545–557. https://doi.org/10.1016/s0016-7037(00)00559-7

Goni, M. A., Thunell, R. C., Woodwort, M. P., & Muller-Karger, F. E. (2006). Changes in wind-driven upwelling during the last three centuries: Interocean teleconnections. *Geophysical Research Letters*, *33*(15), L15604. https://doi.org/10.1029/2006gl026415

Juillet-Leclerc, A., Labeyrie, L. D., Reyss, J. L., & Schrader, H. (1991). Temperature variability in the Gulf of California during the last century—A record of the recent strong El-Nino. *Geophysical Research Letters*, *18*(10), 1889–1892. https://doi.org/10.1029/91gl02284

Juillet-Leclerc, A., & Schrader, H. (1987). Variations of upwelling intensity recorded in varved sediment from the Gulf of California during the past 3,000 years. *Nature*, *329*(6135), 146–149.

Kawabe, I. (1978). Calculation of oxygen isotope fractionation in quartz-water system with special reference to low-temperature fractionation. *Geochimica et Cosmochimica Acta*, *42*(6), 613–621. https://doi.org/10.1016/0016-7037(78)90006-6

Knauth, L. P., & Epstein, S. (1976). Hydrogen and oxygen isotope ratios in nodular and bedded cherts. *Geochimica et Cosmochimica Acta*, *40*(9), 1095–1108. https://doi.org/10.1016/0016-7037(76)90051-x

Labeyrie, L. D., & Juillet, A. (1982). Oxygen isotopic exchangeability of diatom valve silica—Interpretation and consequences for paleo-climatic studies. *Geochimica et Cosmochimica Acta*, *46*(6), 967–975. https://doi.org/10.1016/0016-7037(82)90052-7

Labeyrie, L. D., Juilletleclerc, A., Binz, P., & Decarreau, A. (1988). Oxygen isotopes in biogenic silica and other poorly crystallized hydrated low-temperature minerals. *Chemical Geology*, *70*(1-2), 185–185. https://doi.org/10.1016/0009-2541(88)90743-7

Labeyrie, L. J. (1974). New approach to surface seawater paleotemperatures using O^{18}-O^{16} ratios in silica of diatom frustules. *Nature*, *248*(5443), 40–42.

Leclerc, A. J., & Labeyrie, L. (1987). Temperature dependence of the oxygen isotopic fractionation between diatom silica and water. *Earth and Planetary Science Letters*, *84*(1), 69–74.

Menicucci, A. J., Matthews, J. A., & Spero, H. J. (2013). Oxygen isotope analyses of biogenic opal and quartz using a novel microfluorination technique. *Rapid Communications in Mass Spectrometry*, *27*(16), 1873–1881. https://doi.org/10.1002/rcm.6642

Menicucci, A. J., Spero, H. J., Matthews, J., & Parikh, S. J. (2017). Influence of exchangeable oxygen on biogenic silica oxygen isotope data. *Chemical Geology*, *466*, 710–721. https://doi.org/10.1016/j.chemgeo.2017.07.020

Morley, D. W., Leng, M. J., Mackay, A. W., Sloane, H. J., Rioual, P., & Battarbee, R. W. (2004). Cleaning of lake sediment samples for diatom oxygen isotope analysis. *Journal of Paleolimnology*, *31*(3), 391–401. https://doi.org/10.1023/B:JOPL.0000021854.70714.6b

Moschen, R., Lucke, A., & Schleser, G. H. (2005). Sensitivity of biogenic silica oxygen isotopes to changes in surface water temperature and palaeoclimatology. *Geophysical Research Letters*, *32*(7). https://doi.org/10.1029/2004gl022167

Pride, C. J. (1997). An evaluation and application of paleoceanographic proxies in the Gulf of California, p. 392, University of South Carolina.

Robinson, M. (1973). Atlas of monthly mean sea surface and subsurface temperatures in the Gulf of California. *San Diego Society of Natural History Memoirs*, *5*, 1–97.

Round, F. E., Crawford, R. M., & Mann, D. G. (1990). *Diatoms: Biology and Morphology of the Genera*, (p. 758). Cambridge: Cambridge University Press.

Sancetta, C. (1995). Diatoms in the Gulf of California—Seasonal flux patterns and the sediment record for the last 15,000 years. *Paleoceanography*, *10*(1), 67–84. https://doi.org/10.1029/94pa02796

Schmidt, M., Botz, R., Rickert, D., Bohrmann, G., Hall, S. R., & Mann, S. (2001). Oxygen isotopes of marine diatoms and relations to opal—A maturation. *Geochimica et Cosmochimica Acta*, *65*(2), 201–211. https://doi.org/10.1016/s0016-7037(00)00534-2

Sharp, Z. D., Gibbons, J. A., Maltsev, O., Atudorei, V., Pack, A., Sengupta, S., et al. (2016). A calibration of the triple oxygen isotope fractionation in the SiO_2–H_2O system and applications to natural samples. *Geochimica et Cosmochimica Acta*, *186*, 105–119. https://doi.org/10.1016/j.gca.2016.04.047

Sharp, Z. D., & Kirschner, D. L. (1994). Quartz-calcite oxygen-isotope thermometry—A calibration based on natural isotopic variations. *Geochimica et Cosmochimica Acta*, *58*(20), 4491–4501. https://doi.org/10.1016/0016-7037(94)90350-6

Shemesh, A., Charles, C. D., & Fairbanks, R. G. (1992). Oxygen isotopes in biogenic silica—Global changes in ocean temperature and isotopic composition. *Science*, *256*(5062), 1434–1436. https://doi.org/10.1126/science.256.5062.1434

Spero, H. J., Mielke, K. M., Kalve, E. M., Lea, D. W., & Pak, D. K. (2003). Multispecies approach to reconstructing eastern equatorial Pacific thermocline hydrography during the past 360 kyr. *Paleoceanography*, *18*(1), n/a. https://doi.org/10.1029/2002pa000814

Swann, G. E. A., & Leng, M. J. (2009). A review of diatom delta O-18 in palaeoceanography. *Quaternary Science Reviews*, *28*(5-6), 384–398. https://doi.org/10.1016/j.quascirev.2008.11.002

Swann, G. E. A., Leng, M. J., Sloane, H. J., & Maslin, M. A. (2008). Isotope offsets in marine diatom delta(18)O over the last 200 ka. *Journal of Quaternary Science*, *23*(4), 389–400. https://doi.org/10.1002/jqs.1185

Swann, G. E. A., Maslin, M. A., Leng, M. J., Sloane, H. J., & Haug, G. H. (2006). Diatom delta(18)O evidence for the development of the modern halocline system in the subarctic Northwest Pacific at the onset of major northern hemisphere glaciation. *Paleoceanography*, *21*(1), n/a. https://doi.org/10.1029/2005pa001147

Taylor, N. J. (1985). Silica incorporation in the diatom *Cosinodiscus granii* as affected by light intensity. *British Phycological Journal*, *20*(4), 365–374. https://doi.org/10.1080/00071618500650371

Thunell, R., Pride, C., Tappa, E., & Mullerkarger, F. (1993). Varve formation in the Gulf of California—Insights from time-series sediment trap sampling and remote-sensing. *Quaternary Science Reviews*, *12*(6), 451–464. https://doi.org/10.1016/s0277-3791(05)80009-5

Thunell, R., Pride, C., Ziveri, P., MullerKarger, F., Sancetta, C., & Murray, D. (1996). Plankton response to physical forcing in the Gulf of California. *Journal of Plankton Research*, *18*(11), 2017–2026. https://doi.org/10.1093/plankt/18.11.2017

Thunell, R., Tappa, E., Pride, C., & Kincaid, E. (1999). Sea-surface temperature anomalies associated with the 1997–1998 El Nino recorded in the oxygen isotope composition of planktonic foraminifera. *Geology*, *27*(9), 843–846. https://doi.org/10.1130/0091-7613(1999)027<0843:sstaaw>2.3.co;2

Thunell, R. C. (1998). Seasonal and annual variability in particle fluxes in the Gulf of California: A response to climate forcing. *Deep-Sea Research Part I-Oceanographic Research Papers*, *45*(12), 2059–2083. https://doi.org/10.1016/s0967-0637(98)00053-3

Thunell, R. C., Pride, C. J., Tappa, E., & Mullerkarger, F. E. (1994). Biogenic silica fluxes and accumulation rates in the Gulf of California. *Geology*, *22*(4), 303–306. https://doi.org/10.1130/0091-7613(1994)022<0303:bsfaar>2.3.co;2

Verdugo-Diaz, G., & Garate-Lizarraga, I. (2018). Distribution of functional groups of phytoplankton in the euphotic zone during an annual cycle in Bahia de La Paz, Gulf of California. *CICIMAR Oceanides*, *33*(1), 47–61.

Verdugo-Diaz, G., Martinez-Lopez, A., Gaxiola-Castro, G., & Valdez-Holguin, J. E. (2012). Phytoplankton photosynthetic parameters from the Gulf of California southern region. *Revista De Biologia Marina Y Oceanografia*, *47*(3), 527–535. https://doi.org/10.4067/s0718-19572012000300014

Waelbroeck, C., Mulitza, S., Spero, H., Dokken, T., Kiefer, T., & Cortijo, E. (2005). A global compilation of late Holocene planktonic foraminiferal delta O-18: Relationship between surface water temperature and delta O-18. *Quaternary Science Reviews*, *24*(7-9), 853–868. https://doi.org/10.1016/j.quascirev.2003.10.014

Webb, E. A., & Longstaffe, F. J. (2000). The oxygen isotopic compositions of silica phytoliths and plant water in grasses: Implications for the study of paleoclimate. *Geochimica et Cosmochimica Acta*, *64*(5), 767–780. https://doi.org/10.1016/s0016-7037(99)00374-9

Wejnert, K. E., Pride, C. J., & Thunell, R. C. (2010). The oxygen isotope composition of planktonic foraminifera from the Guaymas Basin, Gulf of California: Seasonal, annual, and interspecies variability. *Marine Micropaleontology*, *74*(1-2), 29–37. https://doi.org/10.1016/j.marmicro.2009.11.002

Zheng, Y. F., Metz, P., Satir, M., & Sharp, Z. D. (1994). Oxygen-isotope fractionation between calcite and forsterite formed via reaction from dolomite and tremolite at 680-degrees-C. *European Journal of Mineralogy*, *6*(2), 179–186. https://doi.org/10.1127/ejm/6/2/0179